

FR9401590

I.P.N. - 91406 ORSAY CEDEX

CNRS - IN2P3 UNIVERSITÉ PARIS - SUD

institut de physique nucléaire



IPNO 93 - 06

**"Activities on cryostats and SRF cavities
at the I.P.N. Orsay laboratory"**

S. BÜLHER, A. CARUETTE, M. FOUAIDY, T. JUNQUERA

**Presented at the 6th Workshop on RF superconductivity,
CEBAF (Newport News, Oct. 1993)**

IPNO 93 - 06

**"Activities on cryostats and SRF cavities
at the I.P.N. Orsay laboratory"**

S. BÜLHER, A. CARUETTE, M. FOUAIDY, T. JUNQUERA

**Presented at the 6th Workshop on RF superconductivity,
CEBAF (Newport News, Oct. 1993)**

**ACTIVITIES ON CRYOSTATS AND SRF CAVITIES
AT THE IPN ORSAY LABORATORY**

S. BUHLER, A. CARUETTE, M. FOUAIDY, T. JUNQUERA

Institut de Physique Nucléaire (CNRS - IN2P3), 91406 ORSAY Cedex (France)

Abstract

The main effort of the SRF community at Orsay during the last five years was concentrated on the MACSE project (study, construction, assembly and test of 3 cryostats), participation to the TESLA project and R & D activities in close collaboration with the Saclay SRF group. In this paper, 3 major topics will be outlined and briefly discussed : cryogenics, scanning surface thermometers for diagnostics on SRF cavities and thermal behaviour analysis of HOM couplers. The main results obtained in this frame since the 5th SC workshop at Hamburg in 1991 will be presented.

I - CRYOGENICS

Since 1986 a small group (4 to 10 people) from IPN Orsay has participated, essentially on a part-time basis, with cryogenic and R & D activities on the MACSE (Maquette d'Accélérateur à Cavités Supraconductrices pour Electrons) and TTF (Tesla Test Facility) projects. A test facility has been built at Orsay which allows basic cryogenic experimentation with vertical test cryostats (Ø 270 and Ø 350 mm) and preliminary test runs of the cavity cryostats with a refrigeration power of up to ≈ 5 W at 1.8 K with LHe supplied from the University central liquefier.

1. MACSE PROJECT COLLABORATION

1.1. Cryostat design for cryomodules cm-0/1/2

Two types of cryostat have been designed : a single cavity module for the capture cryostat CM-0 (Fig. 1) and a four cavity arrangement for the cryomodules CM-1/2, [1], [2], [3].

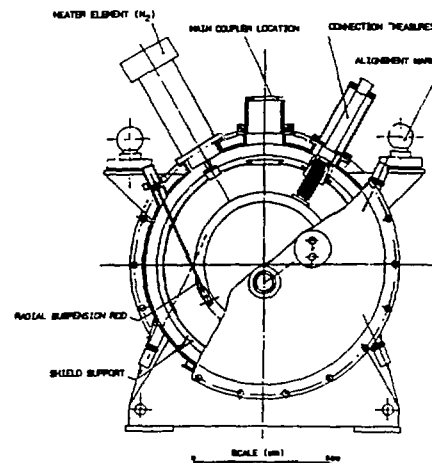
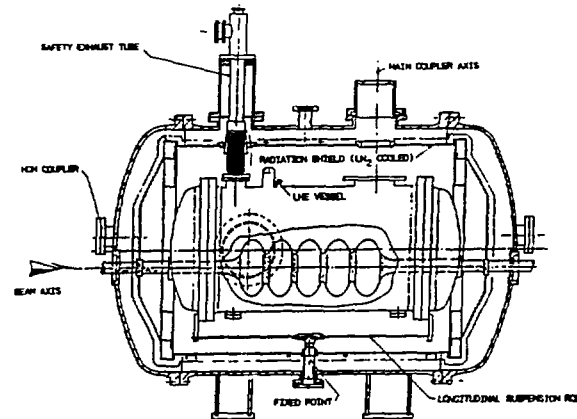


Fig. 1 : Cryomodule MACSE CM-0 (capture cryostat)

1.2. Cryogenic tests

A preliminary test of the completed cryostat, still without any cavity, allowed several interesting investigations :

- Measure of the static heat loads for the LHe vessel and the radiation shield (§ 1.2.1.).

- Discrimination of the heat flux to the radiation shield with a differential analysis of the experimental results from CM-O and CM-2.

- Estimate of a likely "radiation leak" from ambient temperature into the LHe vessel with an electrically heated vacuum tank up to 340 K (§ 1.2.2.).

- Recording of TAO (Thermal Acoustic Oscillations) and experiences with different damping devices.

1.2.1. Static heat load on cryomodules

As the measured static heat load in the LHe vessel was higher than that estimated (Table I), a suspected "radiation leak" through a provisional MLI insulation was demonstrated experimentally (§ 1.2.2.).

HEAT FLOW RATE		LOCATION	NUMERICAL VALUES	
$T_e + T_w$ (K)	Mode #		ESTIMATE (W)	MEASUREMENTS (W)
300 + 80	R	Vacuum tank + 80 K shield with MLI	71	112 ± 3
	R	Vacuum tank + baffles	37	
	C	Shield supports	7	
	R+C	Beam tube	3	
	C	80 K heat intercepts	11	
300 + 4 or 80 + 4	R	Radiation shield + LHe vessel	0.5	7..10 (37..43)
	C	Suspension rods	0.15	
80 + 4	R+C	Beam tube	0.30	5.35 (6.15)≡
	C	Neck tubes + control wires	3.3	
	C	HM connection	1.1	
	C	Main coupler	0.89	

LEGEND :
 # Transmission Mode : C = Conduction; P = Radiation
 ≡ Main coupler included (not mounted for tests IPW)
 ≡≡ TAO = Thermal Acoustic Oscillations

Table I : Static heat load for cryomodule CM-2

1.2.2. Measurement of a radiation leak

Under steady state conditions, the total heat flow \dot{Q}_{tot} into a LHe vessel or in a LN cooled radiation shield is evaluated from the boil-off rate M of the refrigerant (LHe or LN) and the measured temperature of its cold vapour at the outlet interface.

For a cryostat of a given geometry we observe two kinds of heat flow from the temperature T to T_0 :

- Conduction heat flow $\dot{Q}_C = \text{Const}(C) \cdot \int_{T_0}^T \lambda \cdot dT$

- Radiation heat flow $\dot{Q}_R = \text{Const}(R) \cdot (T^4 - T_0^4)$

- Total heat flow $\dot{Q}_{tot} = \dot{Q}_C + \dot{Q}_R$

Let us consider a LHe vessel (Fig. 2) thermally protected with a LN cooled shield which intercepts radiation and conduction heat at the shield temperature, T_s . In standard operation, the vacuum tank stays normally at ambient temperature $T = T_1$, but with an electric heater applied we can easily raise T to a higher value T_2 . Basically, such a

variation has no influence on the heat flow \dot{Q}_{LHe} since the radiation shield at the constant temperature T_s intercepts the higher heat flow from the surroundings, excepting the "radiation leak" \dot{Q}_{RL} which goes through.

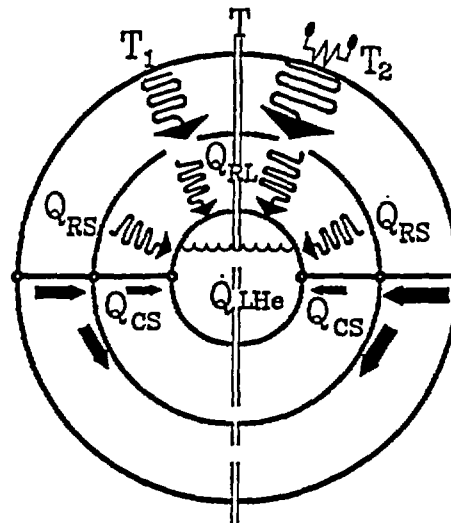


Fig. 2

From the measured heat loads \dot{Q}_{LHe} for two stationary configurations (1) and (2) we can therefore evaluate a possible "radiation leak" as follows :

$$\dot{Q}_{LHe}(1) = \dot{Q}_{CS}(T_s) + \dot{Q}_{RS}(T_s) + \dot{Q}_{RL}(T_1)$$

$$\dot{Q}_{LHe}(2) = \dot{Q}_{CS}(T_s) + \dot{Q}_{RS}(T_s) + \dot{Q}_{RL}(T_2)$$

$$\begin{aligned} \Delta \dot{Q}_{LHe}(1 \rightarrow 2) &= \dot{Q}_{RL}(T_1) - \dot{Q}_{RL}(T_2) \\ &= \text{Const}(RL) \cdot (T_1^4 - T_2^4) \end{aligned}$$

where:

$\dot{Q}_{LHe}(1)$: Total heat flow into LHe with vacuum vessel temperature $T = T_1$

$\dot{Q}_{LHe}(2)$: Total heat flow into LHe with vacuum vessel temperature $T = T_2$

\dot{Q}_{CS} : Conduction heat flow from shield to LHe ($T_S \rightarrow T_O$)

\dot{Q}_{RS} : Radiation heat flow from shield to LHe ($T_S \rightarrow T_O$)

\dot{Q}_{RL} : "Radiation leak" flow
from ambient temperature through shield to LHe ($T \rightarrow T_O$)

With the measured $\Delta \dot{Q}_{LHe}(1 \rightarrow 2)$ we are now able to calculate:

$$\text{Const(RL)} = \frac{\Delta \dot{Q}_{LHe}(1 \rightarrow 2)}{T_1^4 - T_2^4}$$

and finally, the RADIATION HEAT LEAK

$$\dot{Q}_{RL}(1) = \text{Const(RL)} \cdot T_1^4$$

CONFIGURATION	1	← DIFFERENCE →	2
Vacuum vessel temperature	$T_1 = 292$		$T_2 = 326$
Total measured heat load into LHe	$\dot{Q}_{LHe} = 8.84 \text{ W}$	$\Delta \dot{Q}_{LHe}(1 \rightarrow 2) = 1.06 \text{ W}$	$\dot{Q}_{LHe} = 9.90 \text{ W}$
Radiation leak : Const (RL)		$2.633 \cdot 10^{-4} \text{ W.K}^{-4}$	
RADIATION LEAK	$\dot{Q}_{RL} = 1.91 \text{ W}$		$\dot{Q}_{RL} = 2.97 \text{ W}$

Table II : Radiation heat leak measurements on cryomodule CM-2

2. TTF PROJECT COLLABORATION

For this project, in collaboration with DESY, the cryogenic group is in charge of :

- Design and construction of the capture cryostat CRYOCAP (the cavity in its LHe tank and the RF couplers will be supplied from DESY),

- First cryogenic test (without RF) of the fully equipped CRYOCAP at IPN Orsay,

- Second cryogenic test of CRYOCAP with RF on a beam produced from the associated LAL injector on the MACSE location at Saclay.

2.1. CRYOCAP design

The capture cryostat is an element of the injector, a part of the French contribution for TTF. Fig. 3 shows CRYOCAP in its present state of design.

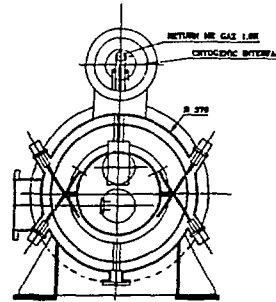
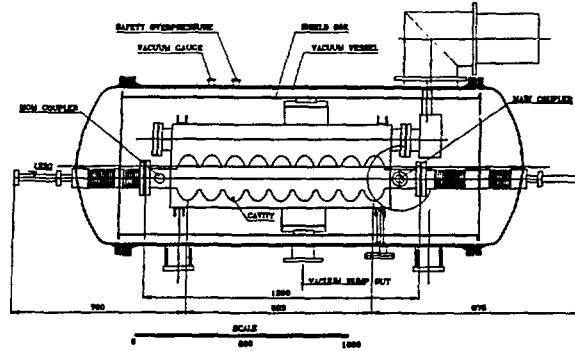


Fig. 3 : Capture cryostat for TTF (10/93)

2.2. Process for cryogenic tests of CRYOCAP

An ancillary but autonomous equipment is designed for preliminary cryogenic tests of the capture cryostat ("CRYOCAP") at two different locations in France prior to its delivery to DESY.

2.2.1 Interfaces for CRYOCAP

- Continuous LHe feed for a LHe bath with a refrigeration power of up to 5 W, stabilized at 1.8 K at a pressure of $16 \pm 0.5 \text{ mbar}$,

- Temperature controlled LN supply for cooling of a 80 K radiation shield,

- LHe cooled heat intercepts at 4.5 K level.

2.2.2. Cryogenic test set up

Fig. 4 shows the layout for the cryogenic process which includes the following refinements :

- Permanent LHe feed from a conventional storage dewar through a LN shielded transfer line,
- Subcooled LHe (4.2 K / 1.2 bar) refrigerates the 4.5 K heat intercepts,
- Heat exchanger E1 (4.2 → 2.2 K) reduces the flash losses of the J.T. expansion of LHe from 1000 to 16 mbar. A by-pass is provided for initial cool-down,
- An economiser cycle with an efficient enthalpy recovery in the 4/80 K region (heat exchangers E20/21) substantially reduces the LHe feed from the storage dewar for the same refrigeration power,
- Complete warm-up of the cold He and N₂ vapours is roughly achieved in two heat exchangers E3 and E4, the latter equipped with an associated heater.

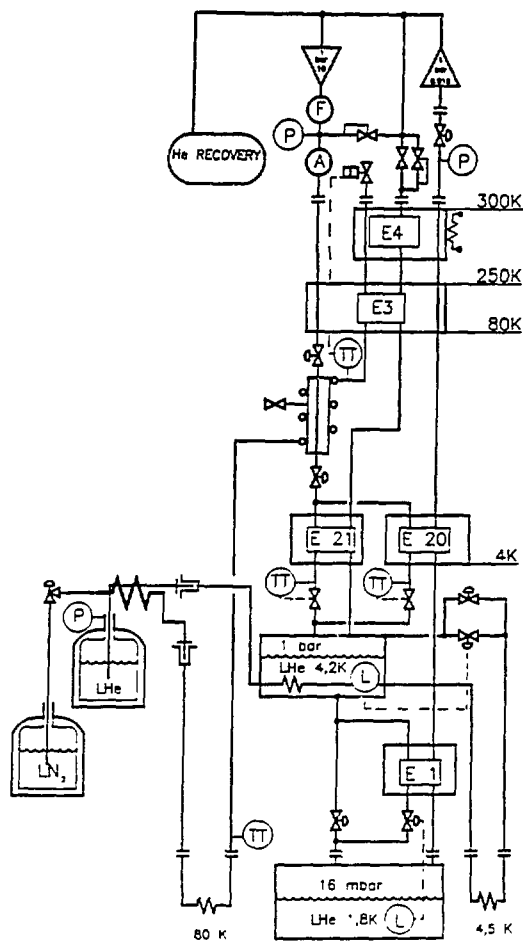


Fig 4 : Test set up for CRYOCAP

II - SCANNING SURFACE THERMOMETERS FOR DIAGNOSTICS ON SRF CAVITIES

The development of superfluid helium cooled scanning surface thermometers for their use as diagnostic probes on monocell and multicell SRF cavities has been continued at Orsay. The new scanning thermometric arm used on 1.5 GHz tri-cell cavities of the GECS is presented on Fig. 5. The new thermometers developed has been greatly improved as compared to those of the first generation [4 - 5] : reduced size from 10 mm down to 6 mm external diameter thus allowing a higher spatial resolution, better mechanical guiding into the rotating thermometric arm giving a better thermal contact with the cavity wall and finally an improved reliability due to a well controlled fabrication process. The thermometer principle remains the same as that of the old generation of "epoxy thermometers" : it consists of an Allen-Bradley carbon resistor housed into a silver block equipped with a sensor tip for the thermal contact to the cavity wall and thermally insulated from the superfluid helium bath by means of an epoxy envelope moulded around the silver block. However, they present two main differences with the first generation as shown in Fig. 6 : thermal anchoring of the sensor manganin wires around the silver block thus reducing the heat leaks to the surrounding He II and the use of a metallic support for the thermometer mounting on the rotating arm. Two models of these epoxy isolated scanning thermometers (Fig. 7) were developed according to this principle : the first one for the 1.5 GHz 3 - cell cavities of the GECS with 10 mm external diameter and the second one for the CERN which are used on 1.5 GHz niobium sputter coated copper SRF cavities [6].

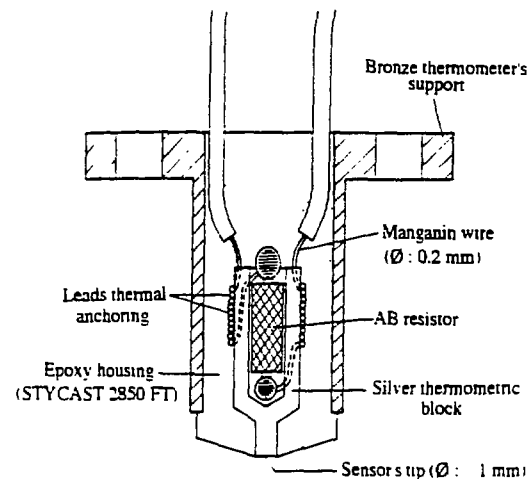


Fig. 6 : Cross-section of a superfluid helium cooled scanning surface thermometer

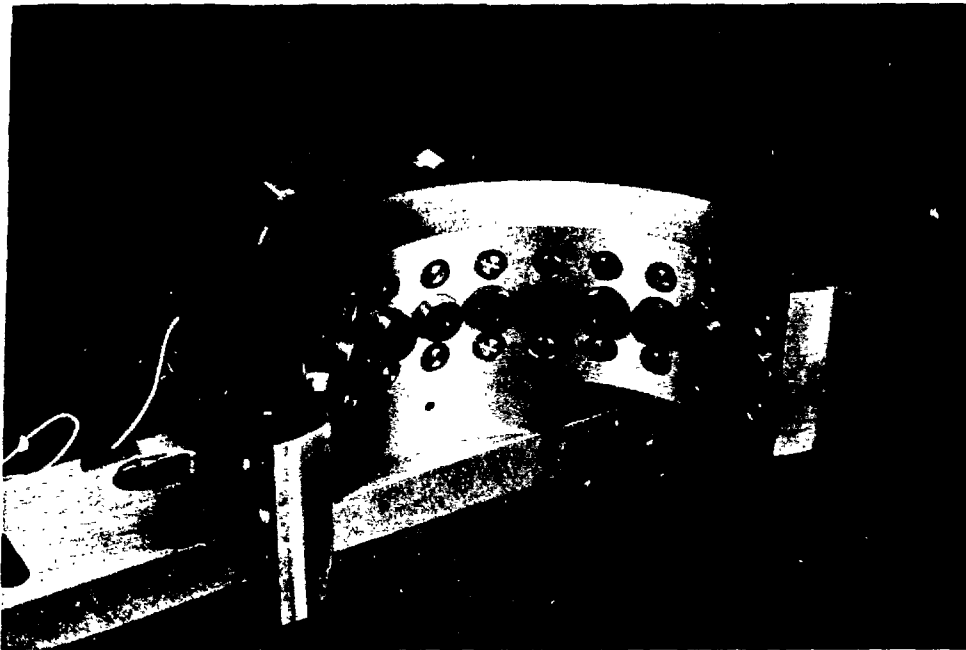
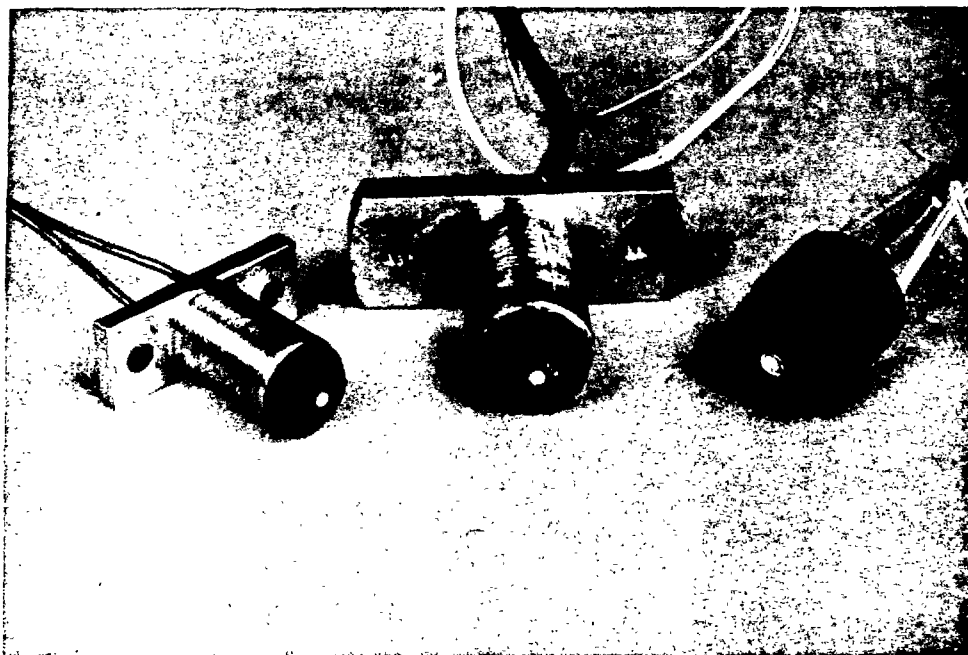


Fig. 5 : Scanning thermometric arm for a 1.5 GHz tri-cell cavities of the GECS



**Fig. 7 : Epoxy thermometers developed at IPN Orsay
for surface temperature measurement in superfluid helium**

- A - Scanning thermometers developed for the CERN (left),**
- B - Scanning thermometers developed for the GECS (center),**
- C - Fixed thermometers developed for the GECS (right)**

In order to study the effect of the insulating envelope size reduction and leads thermal anchoring on the sensitivity of the thermometers developed for the CERN, a set of 13 sensors was calibrated using a special chamber with a heated Nb plate as test specimen and following the experimental procedure described in a previous paper [5]. The thermal response ΔT was measured as function of the heater power at different bath temperature T_{bath} in saturated superfluid helium as well as in subcooled normal helium (i.e. $T_{\text{bath}} > T_{\lambda} = 2.176 \text{ K}$) under 1 atm bath pressure. The calibration results are summarized in the following. An example of the mean thermal response ΔT of these 13 thermometers versus the heater power P is shown in Fig. 8 for $T_{\text{bath}} = 1.52 \text{ K}$ confirming clearly their good linearity. In order to compare their individual thermal response, a typical histogram of these 13 sensors tested simultaneously at $T_{\text{bath}} = 1.52 \text{ K}$ and $P = 388 \text{ mW}$ heater power is presented in Fig. 9. A mean thermal response ($\Delta T = 59.6 \text{ mK}$) was obtained. More precisely, this heater power corresponds to a theoretical heat flux density $q = 30 \text{ mW/cm}^2$ on the cooled side of the Nb specimen if the expression $H_K = 0.043T_{\text{bath}}^{3.18} = 0.163 \text{ W/cm}^2 \cdot \text{K}$ is used for the Kapitza conductance at Nb - He II interface. Consequently, we obtain a mean sensitivity of $2 \text{ mK/mW} \cdot \text{cm}^2$ at $T_{\text{bath}} = 1.52 \text{ K}$.

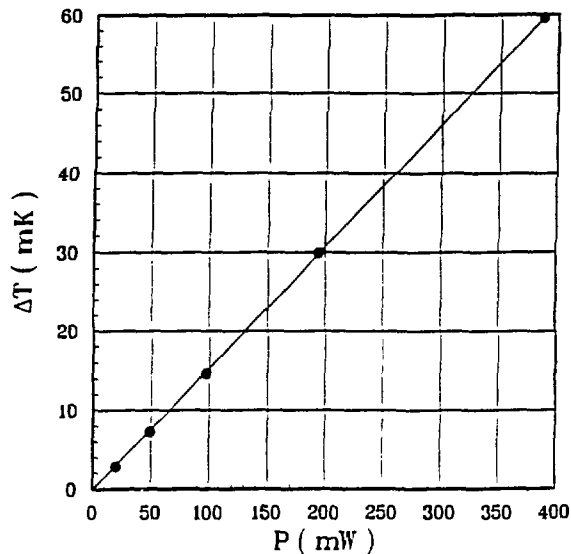
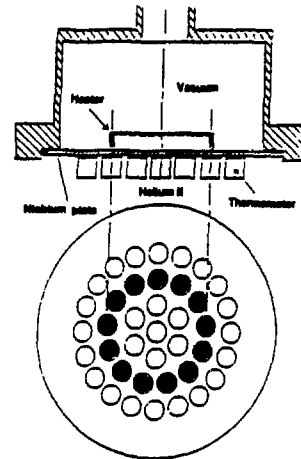


Fig. 8 : Mean thermal response of 13 thermometers versus the heater power ($T_{\text{bath}} = 1.52 \text{ K}$)



Calibration assembly for the epoxy thermometer array

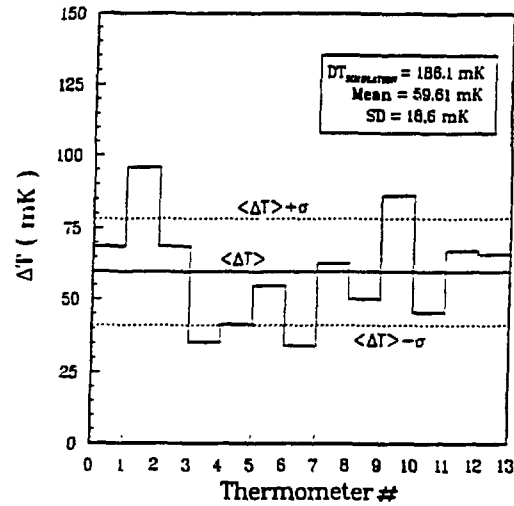


Fig. 9 : A typical histogram in superfluid helium bath ($T_{\text{bath}} = 1.52 \text{ K}$, heater power = 388 mW)

This sensitivity could be compared to the heating ΔT_{RF} induced by RF losses within a niobium plate of $25 \text{ n}\Omega$ surface resistance and subjected to 1000 Gauss (i.e. $E_{\text{acc}} = 25 \text{ MV/m}$) surface magnetic field: the theoretical resulting ΔT_{RF} is 16 mK with RF losses $q_{\text{RF}} = 8 \text{ mW/cm}^2$. One can conclude that such RF losses are easily detectable with these thermometers. Moreover, the observed standard deviation in the previous histogram ($\sigma = 18.6 \text{ mK}$) could be attributed to mechanical mounting problems and the unavoidable presence of He II microchannels inside the Apiezon N grease used as thermal bonding agent between the thermometer tip and the Nb specimen. As expected, the thermal response in superfluid helium is much smaller than in subcooled normal helium bath (Fig. 10): for $T_{\text{bath}} = 2.5 \text{ K}$ and $P = 98 \text{ mW}$ a mean thermal response of 548 mK is obtained with a smaller relative dispersion. This higher sensitivity in subcooled normal helium is due to the poor heat transfer coefficient h at the Nb - LHe interface as compared to the Kapitza conductance H_K .

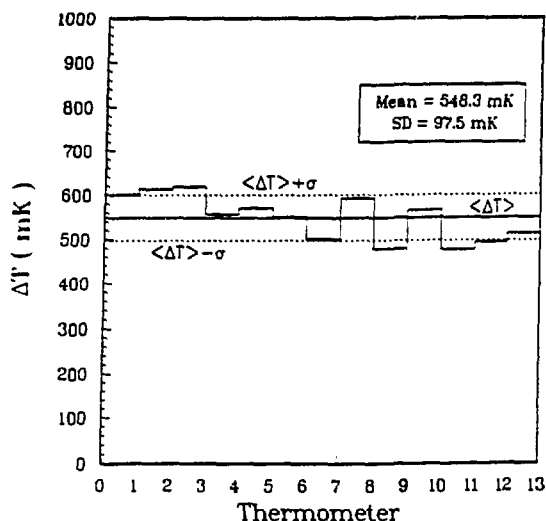


Fig. 10 : A typical histogram in subcooled normal helium bath ($T_{\text{bath}} \approx 2.5$ K, heater power = 97.5 mW, bath pressure = 1 atm)

Indeed, at low heat flux density the heat transfer regime is by natural convection with $h \approx 0.01$ W/cm².K which is at least an order of magnitude smaller than HK . But on the contrary, the resulting spatial resolution is lower than in superfluid helium due to a more important radial heat diffusion (normal helium case). The effect of bath temperature in superfluid helium was extensively studied at a fixed heater power $P = 388$ mW. The results are summarized in table III : as expected ΔT vs T_{bath} , at a fixed P , follows a power law (i.e. $\Delta T \propto T_{\text{bath}}^{-n}$) with an exponent n ranging from 3.4 to 5.6 for $1.5 \text{ K} \leq T_{\text{bath}} \leq 2.0$ K.

Th #	n	C
1	3.38	282.26
2	4.12	541.85
3	5.20	607.31
4	4.04	193.89
5	5.13	357.50
6	3.82	271.31
7	4.55	232.10
8	4.21	365.65
9	4.73	363.11
10	3.77	414.51
11	4.73	325.11
12	5.59	712.08
13	4.38	413.88

$$\Delta T = C \cdot T_{\text{bath}}^{-n}$$

(mK) (K)

Table III : Bath temperature dependence of Orsay thermometers developed for the CERN SRF Group

Notice that these results show a weaker T_{bath} dependence than that previously observed with epoxy thermometers [4][5]. Moreover the small departure from the expected Kapitza exponent (i.e. $3 \leq n \leq 4$) may be due to the complex phenomena inside the bonding agent sandwiched between the sensor tip and the Nb cooled wall. A computer code POISNL [5], based on a finite element method, was used to calculate the temperature distribution within the niobium test specimen and thus to estimate the thermometer efficiency. We recall that the thermometer efficiency η is defined as the ratio of the experimental thermal response ΔT_{Exp} (with respect to T_{bath}) to the simulated temperature jump ΔT_{Sim} at the Nb - He II interface. The results of this numerical simulation along with the deduced η values are summarized in table IV where numerical runs conditions are precised.

T_{bath} (K)	ΔT_{Sim} (mK)	$\Delta T_{\text{Exp}}^{\text{Mean}}$ (mK)	η (%)	$\Delta T_{\text{Exp}}^{\text{Best}}$ (mK)	η (%)
1.52	186.1	59.6	32.0	95.6	51.4
1.70	130.4	37.0	28.4	61.3	47.0
1.90	98.9	22.7	23.0	38.2	38.6

For numerical simulation, the following expression of the Kapitza conductance at Nb - He II interface was used :

$$HK \text{ (W/cm}^2\text{.K)} = 0.043 T_{\text{bath}}^{3.18} f(\Delta T)$$

ΔT_{Sim} : simulated thermal response

$\Delta T_{\text{Exp}}^{\text{Mean}}$: mean thermal response of an array of 13 thermometers

$\Delta T_{\text{Exp}}^{\text{Best}}$: thermal response of the best thermometer (runs of July 12, 1993)

Table IV : Measurement efficiency of Orsay thermometers developed for the CERN SRF Group

The observed η values computed with the mean thermal response of the 13 thermometers increase from 23 % ($T_{\text{bath}} = 1.9$ K) up to 32 % ($T_{\text{bath}} = 1.52$ K). Notice that this mean efficiency is a factor ≈ 1.5 higher than that previously reported [5] for epoxy thermometers (10 mm external diameter) at $T_{\text{bath}} = 1.7$ K. The "best" thermometer has a very good sensitivity : $\eta = 51$ % at $T_{\text{bath}} = 1.52$ K. In conclusion, all these results confirm the improvement of the fabrication process, reliability and good sensitivity of these new thermometers even with an important size reduction of the epoxy envelope. These thermometers have been already used at CERN on 1.5 GHz niobium sputter coated cavities with good results [6]. Finally, we are working in collaboration with DESY for the use of such thermometers ("CERN type") as diagnostics probes on 1.3 GHz 9 cell TESLA cavities which will be equipped with ≈ 130 thermometers.

III - KAPITZA CONDUCTANCE AT NIOBIUM - HE II INTERFACE

The special test cell (Fig. 11) developed [5] for the calibration of the vacuum thermometers designed for accurate surface temperature measurement in superfluid helium is used to measure the Kapitza conductance H_K for niobium specimen with the same surface preparation as for SRF cavities.

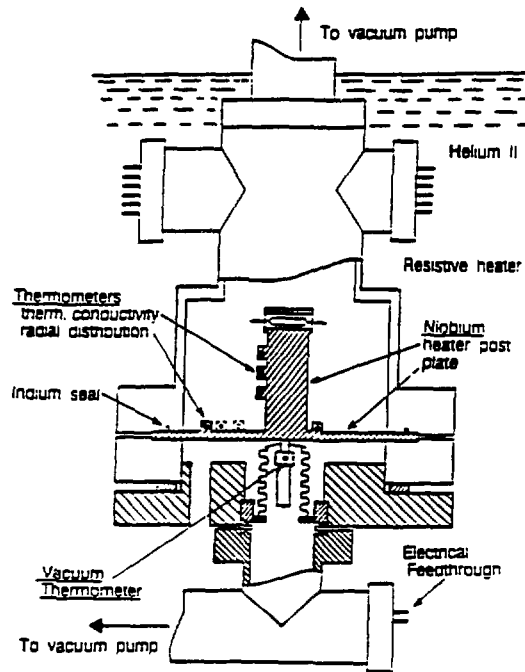
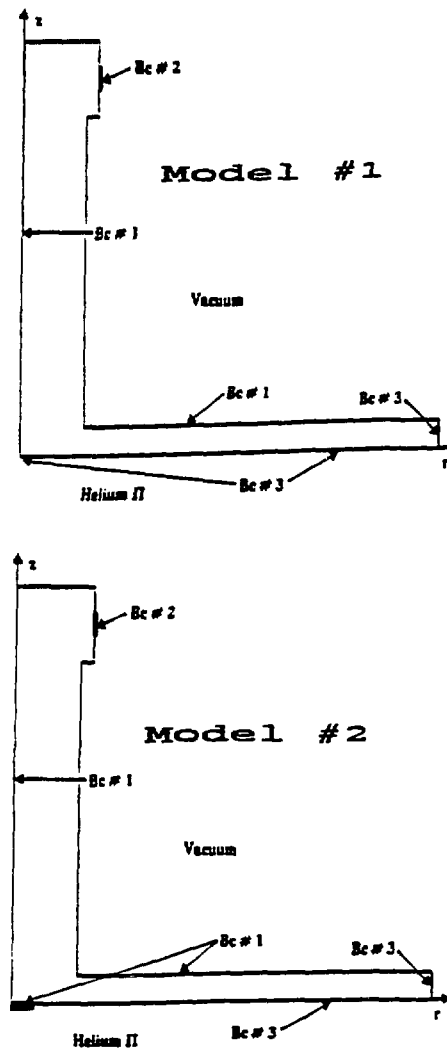


Fig. 11 : Vacuum thermometer's calibration cell

The niobium plate-heater assembly is machined out from niobium ingot (RRR = 270). It is equipped with three resistive thermometers (Th1 - Th3) located on the heater post for in situ thermal conductivity measurement and four other thermometers (Th4 - Th7) to measure the radial temperature distribution on the niobium plate hot side. The detailed experimental procedure has been previously described [5]. The temperature distribution within this Nb specimen was computed with the POISNL code. As the thermal conductivity $k(T)$ is measured in situ with this cell, the Kapitza conductance H_K at Nb - He II interface remains the only unknown parameter of the problem. Thus its value could be adjusted by fitting the experimental temperature distribution within the Nb specimen to the numerical simulation results computed by POISNL. A trial and error method was adopted for this purpose [5]. For the boundary conditions at the thermometer location (cold side of the niobium), two models (Fig. 12) has been considered.



Boundary conditions :

Bc # 1 : adiabatic wall

Bc # 2 : prescribed heat flux density

Bc # 3 : heat transfer at Nb - He II interface controlled by the Kapitza conductance H_K

Fig. 12 : The two simulation models used

In the model # 1, the effect of the thermometer on the cooling conditions at its location is ignored. Consequently, the heat transfer in this region (i.e. thermometer tip location) is controlled by the Kapitza conductance H_K at Nb - He II interface. In the model # 2, the thermometer tip is assumed to hide locally and perfectly the niobium wall at its location. As the sensor is adiabatic (vacuum insulation), this region which is then practically unwetted by superfluid helium may be considered as thermally insulated from the He II bath. An example of H_K adjustment using this method is shown on Fig. 13 where the experimental data are compared to numerical simulation results obtained with these two models.

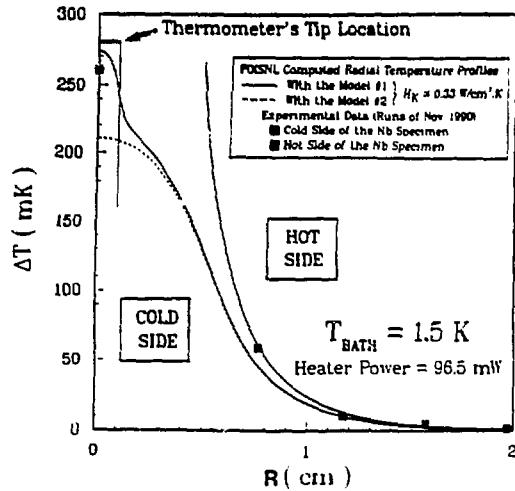


Fig. 13 : Example of Kapitza conductance adjustment

The radial temperature distribution are presented for both cold and hot side of the niobium specimen at $T_{\text{bath}} = 1.5 \text{ K}$ for 96.5 mW heater power. The relative difference between experimental data and numerical simulation results is less than 20 %, thus showing a good agreement. The model # 1 leads to a thermometer efficiency higher than 100 %. Consequently, the model # 2 was finally chosen to analyse all the experimental data for T_{bath} varying from 1.5 K up to 2.0 K and a fixed heater power of 96.5 mW. The agreement between experimental data and the computed results was good in the whole temperature range, giving a confidence of H_K adjustment method. The resulting H_K values obtained with this method for 3 different experimental runs, each run covering the whole temperature range 1.5 K - 2.0 K, are summarized in table V where they are compared to previous results reported by other authors [7][8].

Authors	h_c	n	$H_K @ 1.8 \text{ K}$	Runs
Mittag (1973)	0.0170	3.62	0.143	
Mittag (1973)	0.020	4.65	0.308	
Wilkes (1978)	0.0136	3.99	0.142	
Wilkes (1978)	0.0252	3.90	0.242	
Wilkes (1978)	0.0072	4.41	0.096	
Wilkes (1978)	0.0145	3.96	0.140	
Wilkes (1978)	0.0240	4.30	0.310	
IPN-GECS	0.0883	3.25	0.596	Nov 90 (*)
IPN-GECS	0.0774	3.44	0.585	Dec 90 (*)
IPN-GECS	0.0359	4.28	0.444	Oct 91 (**)

$H_K = h_c T_{\text{bath}}^n \text{ (W/cm}^2 \text{ K)}$

(*) Standard SRF Surface Chemical Treatment and Long Term (10 months) stay of the sample under Ambient Atmosphere (Air)

(**) The same sample underwent a new Chemical Treatment in standard way as for item (*) but was kept under helium atmosphere before experimental runs

Table V : Experimental Kapitza conductance H_K for niobium samples of different surface treatments

Table V : Experimental Kapitza conductance H_K for niobium samples of different surface treatments

Concerning our data, we note firstly that the long term (i.e. several months) stay of the sample under ambient atmosphere seems to stabilize H_K value and secondly, as expected, the chemical treatment has a relatively marked effect on this parameter. The exponent n of H_K dependence on T_{bath} ($H_K \propto T_{\text{bath}}^n$) lies within the range of the results previously reported. Finally, our absolute H_K data at 1.8 K are higher than the result published by the other authors, thus confirming the strong dependence of H_K on the specimen surface treatment.

IV - THERMAL BEHAVIOUR ANALYSIS OF HOM COUPLERS FOR SRF CAVITIES

The superconducting Higher Order Modes (HOM) couplers used for SRF cavities cooled by liquid helium (LHe) are often limited by thermal breakdown induced by various dissipative phenomena for accelerating electric fields E_{acc} in the range 2 - 5 MeV/m, when no efficient cooling of the inner conductor is provided. These E_{acc} values are very much smaller than the design values foreseen for future projects (e.g. TESLA [9] : $E_{\text{acc}} = 25 \text{ MeV/m}$). Moreover, in the TESLA design of the cavity - cryostat assembly, all the couplers (main and HOM) as well as the beam tubes are located inside the insulation vacuum of the LHe vessel ; this indirect LHe cooling of the HOM coupler in particular should obviously reduce its thermal quench limit. Consequently, it is necessary to choose properly the HOM coupler geometry and its construction material in order to increase its capability to withstand anomalous RF losses.

At low temperatures all the parameters (thermal conductivity, RF surface resistance, heat transfer coefficient, specific heat) involved in the boundary problem of concern (i.e. heat equation with appropriate boundary and initial conditions) are strongly temperature dependent. The resulting problem is then non linear. Moreover, the system studied is not axisymmetrical, hence a 3D computer code is needed to solve the problem. We used the CASTEM 2000 code [10] for this purpose : this Finite Element Method based code can handle such non linear problems in both transient and steady - state conditions for arbitrarily shaped computational domains including multiple regions (i.e. materials).

This method was already described in details [11 - 12], so we will focus on its application to the HOM coupler.

4.1. The model and thermal stability criteria

The real system studied [11] consists in the beam tube of cavity supporting the HOM coupler, the fish - hook HOM coupler itself (external conductor (diameter : 40 mm), inner conductor (diameter : 8 mm)), the Nb flange of the cryostat tank and the LHe cooled part of the cavity.

For numerical simulation, this system was modelled using a slightly modified geometry (Fig. 14) which includes all the parts described previously up to the first iris of the cavity. Notice however that all the thermal contact resistances at the sealings (i.e. flanges of the HOM coupler) were neglected and the fish - hook has been replaced by a straight inner conductor (IC) which has no influence on the numerical results as thermal radiations are negligible ($T < 10$ K). Finally, the heat flux coming from the RF coaxial cable was also neglected and a simple Nb plate was used instead of the upper part of the HOM.

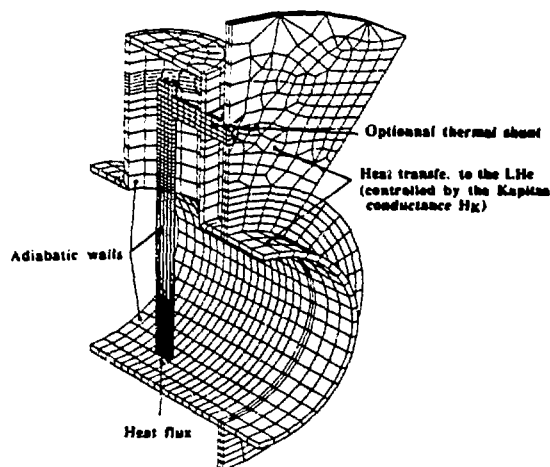


Fig. 14 : Meshed cavity - HOM assembly and applied boundary conditions

In the defect free case, the resulting total normal RF losses dissipated on the IC of the HOM remain lower than 0.4 mW for $T_{\text{bath}} = 2.0$ K, $E_{\text{acc}} = 25$ MeV/m and a residual surface resistance $R_{\text{res}} = 20$ n Ω [12]. These very low RF dissipations cannot then explain an increase of the hot spot temperature beyond the niobium critical temperature $T_c = 9.2$ K. Consequently, anomalous RF dissipation sources (cavity electron loading, high surface resistance defects, multipactor...) have to be considered as possible causes of the HOM coupler thermal breakdown. We have then assumed a highly dissipative area, located at the end of the IC which is the farthest point from the cold source. With this pessimistic assumption, a lower limit of the heat flux Q_c inducing the quench will be obtained.

The thermal stability of such system in steady - state conditions will be ensured if two conditions are fulfilled : the maximum temperature T_{max} at the hot spot must be lower than $T_c = 9.2$ K and the maximum heat flux density transferred to the superfluid helium bath must be lower than the critical heat flux density inducing the film - boiling.

4.2. Steady state regime results

The steady - state temperature distribution in the system was computed up to the critical heat flux (Q_c) for the following arrangements and the results are summarized in TableVI:

1 . the whole HOM coupler - cavity assembly is machined out from bulk niobium with RRR = 40, 194 or 570,

2 . all these parts are in bulk niobium (RRR = 40, 194, or 570) excepted the Inner Conductor and the stub which are made of sputtered niobium onto a copper substrate of RRR = 300,

3 . the same arrangement as in item # 1 but with the addition of a copper (RRR = 300) thermal shunt between the coupler and the LHe cryostat flange,

4 . the same arrangement as in item # 2 but with the addition of the thermal shunt as described in item # 3.

NIObIUM RRR	ARRANGEMENT	CRITICAL HEAT FLUX Q_c (mW)
40	# 1	72
194	# 1	314
570	# 1	925
40	# 2	600
194	# 2	1860
570	# 2	3418
40	# 3	79
194	# 3	347
570	# 3	1017
40	# 4	2700 *
194	# 4	3328 *
570	# 4	5430

TableVI : Critical heat flux inducing the HOM coupler thermal breakdown in the steady - state regime
(*) Quench limited by the transition to film boiling on the LHe cooled Nb flange at 2.4 W/cm² heat flux density

For the first arrangement, the critical heat flux inducing the quench increases nearly in proportion to the RRR (i.e. $\frac{Q_c}{RRR} = 1.8$ W, 1.62 W and 1.62 W for RRR = 40, 194 and 570 respectively). Moreover, the analysis of the temperature profiles along the IC for the arrangements # 1 and # 3 at $Q = Q_c$ shows non-linear effects which increase with the RRR. But the temperature difference across the IC is always around 3.3 K whatever the RRR may be as shown by the isotherms (Fig. 15).

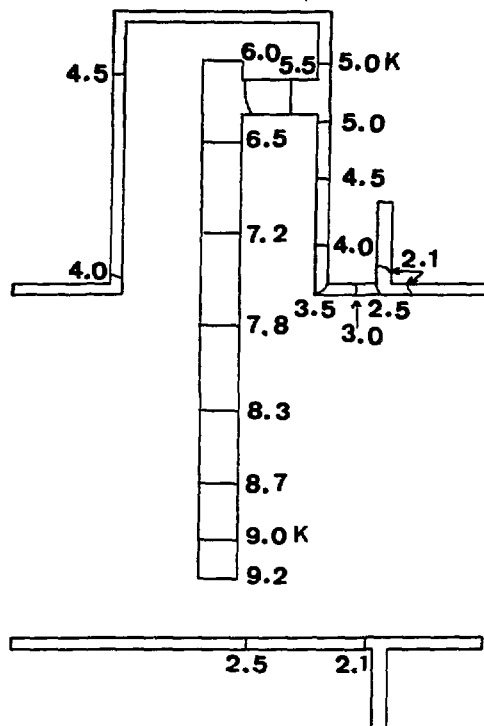


Fig. 15 : CASTEM 2000 computed isotherms for the arrangement # 1 (RRR = 194) with $Q = Q_c = 314$ mW

The comparison of the results obtained with the arrangement # 1 and # 3 shows that the thermal shunt has no sensitive effect on Q_c for a fixed RRR : the system is always limited by the thermal impedance of the IC.

In order to overcome this limitation, the arrangement # 2 was examined : a strong reduction is obtained for the IC thermal impedance R_{th} due to the high thermal conductivity of copper as compared to that of niobium. Once this limitation has been overcome, the effect of the thermal shunt (arrangement # 4) improves greatly Q_c from 3.4 W up to 5.4 W. This gain was due to the small thermal impedance R_{th} of the IC : $R_{th} = 0.6$ K/W which is 6 times smaller than for the best niobium studied (i.e. RRR = 570). In this numerical run (i.e. $Q_c = 5.4$ W, arrangement # 4) 70 % of Q_c is derived through the copper thermal shunt to the cold source (Fig.16).

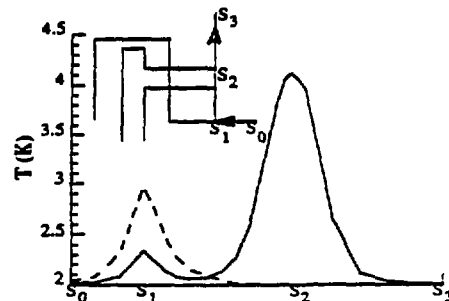


Fig. 16 : Temperature profile along the LHe cooled Nb flange (sketched in the insert)
Full line with thermal shunt ($Q_c = 5.4$ W)
Dashed line : without thermal shunt ($Q_c = 3.4$ W)

4. 2. Transient regime results

This study was limited to the arrangement # 1 with RRR = 194 bulk niobium. The applied heat flux is now pulsed and close to the cycle foreseen for TESLA (pulse length $\tau_p = 2$ ms ; repetition rate $f_{rep} = 10$ Hz). Independently on the applied heat flux, the system reaches a stationary regime in few pulses (≈ 10). More precisely, for $Q_c = 6$ W, the maximum hot spot temperature T_{max} (Fig. 17) increases up to 8.6 K at the end of the first RF pulse (i.e. $t = 2$ ms), does not recover its initial values (i.e. $T_{bath} = 1.8$ K) before the beginning of the second RF pulse ($T = 4.4$ K) and continue to oscillate hence reaching a stationary regime in few pulses where T_{max} oscillates periodically between 6.2 K and 9.2 K.

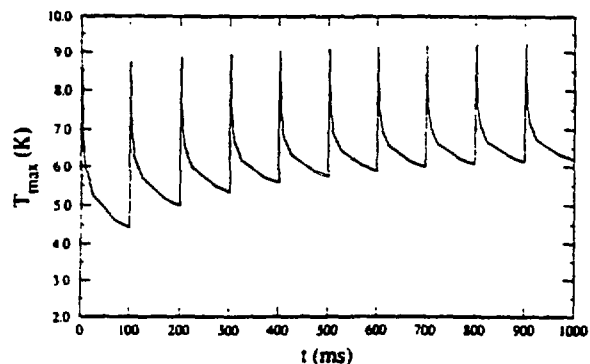


Fig. 17 : Temperature of the hot spot vs time

The higher temperature T_{max} that can be reached at the hot spot after an infinity of RF pulses ($\tau_p = 2$ ms, $f_{rep} = 10$ Hz) was computed as function of the applied heat flux. The resulting temperature difference ΔT_{max} with respect to T_{bath} (i.e. $\Delta T_{max} = T_{max} - T_{bath}$, with $T_{bath} = 1.8$ K) follows a power law versus the heat flux :

$$\Delta T_{max} (K) = 3.63 Q_{(W)}^{0.35} + 0.31 Q_{(W)}^{0.49}$$

A first fish-hook coupler was tested successfully in superfluid helium at $T_{\text{bath}} = 2.0\text{K}$. This HOM coupler was tested on a 1.5 GHz niobium cavity with a stronger TM 010 coupling than that needed in TESLA operation. In CW mode, the HOM coupler sustained a maximum accelerating gradient of $E_{\text{acc}}^{\text{quench}} = 13\text{ MeV/m}$ just before the quench. Notice that this quench level was not sensitive to the Q_{ext} tuning which was varied from $8 \cdot 10^{10}$ ($E_{\text{acc}}^{\text{quench}} = 12.7\text{ MeV/m}$) up to $Q_{\text{ext}} = 2 \cdot 10^{12}$ ($E_{\text{acc}}^{\text{quench}} = 13.5\text{ MeV/m}$).

This HOM coupler was also tested in pulsed mode ($f_{\text{rep}} = 1\text{ Hz}$), the maximum E_{acc} reached was 20.7 MeV/m , limited by the cavity quench, with a duty cycle of $\approx 40\%$. Experimental tests are continued and more detailed results will be presented in a next paper.

In conclusion, a HOM coupler which can theoretically sustain in CW mode heat loads beyond 5 W due to anomalous RF losses is possible by using an IC and stub made with sputtered Nb onto a Cu substrate and adding a copper thermal shunt connecting it to the cryostat Nb flange. In the pulsed mode, the maximum heat loads sustained by the bulk Nb coupler is 6 W . Notice that in all cases, the maximum temperature on the iris of the cavity does not exceed 0.1 K beyond the bath temperature and thus the thermal stability of the cavity is always ensured: the cavity seems to be thermally decoupled from the HOM coupler.

The first experimental results are good and seem to confirm the calculation results. However, a more detailed and extensive experimental data analysis is needed to assess all these results.

REFERENCES

- [1] BUHLER S., "Aspects cryogéniques des cryostats MACSE CM-0 et CM-1", Rapport IPNO 90-06, Orsay, Oct. 1990.
- [2] BUHLER S., "Cryomodules MACSE CM-0 et CM-1, compte rendu des essais IPN", Rapport IPNO 90-08, Orsay, Dec. 1990.
- [3] BUHLER S. "Cryomodule MACSE CM-2 : Calculs et essais IPN du cryostat", Rapport IPNO 91-06, Orsay, Nov. 1991.
- [4] BRIZZI, R. et al., Proceedings of the ASME Heat Transfer Conference, Seattle (USA), June 1990.
- [5] FOUAIDY, M. et al., Proceedings of the 5th Workshop on RF Superconductivity, Hamburg (Germany), August 1991.

- [6] BLOESS, D. et al., this workshop,
- [7] MITTAG, K., Cryogenics 13 (1973) 94,
- [8] WILKES, K.E., Ph D thesis, Ohio State Univ. (1978),
- [9] TESLA collaboration, "A proposal to construct and test prototype superconducting RF structures for linear colliders", DESY, February 1992.
- [10] VERPEAUX, P. et al., Structural mechanics reactor, 10, Los Angeles, (1989),
- [11] CHEL, S., and FOUAIDY, M., "Thermal behaviour of HOM coupler", internal report, CE Saclay, DAPNIA/SEA 93,
- [12] FOUAIDY, M., et al., Proceedings of the IEEE PAC 93, Washington D.C., May 1993.